

FBApro: A fast, simple linear transformation for diverse metabolic modeling tasks

Ariel Bruner, Mona Singh

January 22, 2026

Abstract

Constraint-based metabolic modeling is the predominant framework for simulating cellular metabolism. The central assumption of these models is that metabolism operates at a steady state, meaning that the production and consumption rates of each metabolite are balanced. This assumption imposes linear constraints on the fluxes of biochemical reactions. Flux Balance Analysis (FBA), a fundamental method in the field, is formulated as an optimization problem maximizing a cellular objective (e.g., growth) over the resulting linear subspace of steady state fluxes. Many other methods in the field are expressed either as a modification to FBA, or use FBA as a black box within an algorithm. Here, we propose a simple and general alternative to optimization that, for any flux vector, finds the closest flux distribution within the steady-state subspace. This operation corresponds to an orthogonal projection that enforces the steady-state assumption. We further introduce extensions to handle cases involving unknown or fixed fluxes through modified projections and tailored affine subspaces. The overall approach is computationally efficient, does not require a cellular objective, and is easy to implement. We validate our method and its variants on both synthetic and experimental datasets, demonstrating their speed and utility for denoising and imputing metabolic flux data, and for predicting steady-state fluxes from more readily available types of data.

Code availability: The code implementing FBApro is available at <https://github.com/Singh-Lab/FBApro>. All code required to reproduce the figures in the paper is available, although the data used must be sourced separately. The repository also contains toy models and examples.

1 Introduction

Cellular metabolism is a complex, tightly regulated process that underlies the behavior of biological systems. Modeling metabolism requires characterizing both the biochemical capabilities of organisms, as well as developing computational methods to simulate these processes under specific conditions. Constraint-Based Metabolic Modeling (CBMM) has emerged as a widely-used framework for such simulations. It assumes a steady-state regime in which metabolite concentrations remain constant and reaction fluxes must balance.

CBMM has a long history, with theoretical foundations laid more than 40 years ago. Its most fundamental method is Flux Balance Analysis (FBA) [1–3], which formulates a linear program to capture steady-state flux constraints and an organism-level objective. Large-scale sequencing efforts have enabled the construction of genome-scale metabolic models for numerous organisms [4], and FBA has been instrumental in predicting the metabolic phenotypes of unicellular organisms under various growth conditions [5–8]. Extensions to FBA have also enabled FBA-based predictions of gene knockout effects (e.g., MoMA [9] and ROOM [10]).

Modeling of multi-cellular organisms remains challenging due to heterogeneity across cell types, unclear metabolic objectives, and limited knowledge of *in vivo* metabolite availability. These problems are even more pronounced in the application of CBMM to cancer metabolism, where altered metabolism plays a significant role [11]. The unique challenges of multicellular metabolic modeling, together with the increased availability of 'omics data, have led to the development of numerous methods integrating 'omics data with metabolic models. Gene expression (GE) data are the most widely available, and many algorithms integrate GE with metabolic models to construct context-specific networks or infer context-specific reaction fluxes (e.g. GIMME [12], iMAT [13], MBA [14], INIT [15]), including extensions to incorporate single-cell RNA-seq data (e.g. Compass [16]). Most of these methods formulate optimization problems that incorporate both steady-state constraints and data fidelity terms, often resulting in large linear or mixed-integer programs, sometimes approximated by greedy heuristics. Scaling these approaches to large cohorts or single-cell datasets poses substantial computational challenges.

In parallel, advances in deep learning have enabled breakthrough advances in other areas of computational biology (e.g., [17]), and highlight the value of domain-specific methods that admit closed-form differentiable implementations that can be embedded directly into gradient-based machine learning models. However, to our knowledge, all available CBMM algorithms are based on solving optimization problems, particularly linear and mixed-integer linear programs, which are not easily integrated into end-to-end differentiable pipelines.

Here we present FBAPro, a closed-form linear operation that maps any input assignment of reaction fluxes to the closest steady-state flux vector of the metabolic model under the L_2 metric. FBAPro (short for FBA projection) is based on linear projections, and thus is orders of magnitude faster than FBA while additionally being fully differentiable. Like FBA, FBAPro has a variety of use-cases: GE data integration, where GE of genes for a reaction are used to make initial estimates of fluxes; noise cancellation and data imputation, where noisy and/or missing flux estimates are mapped to steady-state fluxes; simulation of knock-outs, where wild-type fluxes are replaced with zeros for knocked out reactions; and simulating different metabolic objectives, where an objective coefficients vector is treated as flux input. FBAPro is related to previous quadratic programming formulations, such as MoMA, which minimizes the distance of a knockout model steady-state flux from a wild-type reference flux distribution, and the approach of [18] to fit partially measured data. Unlike the aforementioned methods, FBAPro is expressible as a simple orthogonal projection, at the cost of foregoing reaction bounds. While a projection-based steady-state mapping appears in the flux sampling module of the cobrapy metabolic modeling library [19], it has not, to our knowledge, been formally described, generalized, validated, or proposed as an alternative to FBA.

We further introduce two important extensions of FBAPro: FBAProPartial, which projects onto the steady-state space using only a subset of reactions with observed fluxes, and FBAProFixed, which projects while enforcing exact flux values for specified reactions. FBAProPartial is applicable when fluxes are measured for some reactions but information is missing about other reactions, and FBAProFixed is applicable when there are high-confident measurements for a subset of reactions that should not be altered. We show that both FBAProFixed and FBAProPartial can be expressed as a single orthogonal projection to a modified affine subspace of the steady-state space. Moreover, the projection to the modified subspace can be expressed as a function of the subset of reactions with missing (or respectively, exact) values, and not the values themselves. Surprisingly, in the case of FBAProFixed, this is despite the subspace itself being dependent on the actual values, differing between samples. Therefore, when applying the projections to multiple samples from a similar experimental setup, the relevant projection matrix can be precomputed once, and the individual projections are computationally efficient and differentiable.

We validate FBAPro on both simulated and cancer cell line data. On simulated data, we first compare the running time of FBAPro to FBA, iMAT [13], and MoMA [9], and find that FBAPro is orders of magnitude faster. We

compare FBAPro to FBA as it is the *de facto* method for metabolic modeling and has been used in various ways to incorporate gene expression values [20–22]; to iMAT as it is a widely used method for integrating GE with metabolic models to uncover steady state fluxes that are “consistent” with the GE data; and to MoMA as it solves a similarly phrased problem to FBAPro using the traditional optimization approach. The aforementioned methods also have an available implementation written in Python. We then consider simulations where exact, noisy and missing data are derived from steady state fluxes, and demonstrate that the corresponding variants of FBAPro outperform previous approaches in recapitulating the known steady state fluxes. Finally, we consider cancer cell-line gene expression and reaction flux data to show that FBAPro surpasses or has state-of-the-art performance in imputing unmeasured fluxes and mapping gene expression data to the steady-state space while predicting corresponding unseen data. Overall, our results suggest that FBAPro is a flexible, modular and effective approach for high-throughput and large-scale metabolic modeling.

2 Methods

2.1 FBAPro

Assume a metabolic network with m metabolites, r reactions and a stoichiometric matrix $S \in \mathbb{R}^{m \times r}$, such that $S_{i,j}$ is the concentration of metabolite i produced per unit of flux in reaction j . For simplicity, we will ignore the units of these quantities, and additionally ignore bounds on reaction fluxes typically used in such models.

Let $v \in \mathbb{R}^r$ be a representation of fluxes through the network’s reactions. We say that v is a steady-state if $v \in \ker(S)$. Given input values for v , termed the reference fluxes, we are interested in the closest steady-state flux vector. FBAPro is thus the orthogonal projection to the steady-state space, solving

$$\text{FBAPro}(v) = \operatorname{argmin}_{x \in \ker(S)} \|v - x\|_2.$$

While expressed here as a quadratic optimization problem, an orthogonal projection to a linear space is a linear transformation. For any matrix T , let T^+ denote the pseudo-inverse of T , also known as the Moore–Penrose inverse, commonly used in the context of solving least-square data fitting problems. Given T, b and the problem of solving $Tx = b$ for x , we have that T^+b is a solution if one exists, and otherwise is an assignment that minimizes the error $\|Tx - b\|_2$. Similarly, one can think of T^+ as an approximate solution to $TX = I$, or an approximate inverse of T (which can be singular or, as in our case, non-rectangular). An orthogonal projection to the column-space of T , the span of the columns of T , can be expressed as the matrix TT^+ . We refer the reader to [23] for more details on expressing orthogonal projections using the pseudo-inverse.

In this case, the desired projection is to the kernel, or null-space, of S . The null-space of S is orthogonal to the row-space of S , and the row-space of S is the column-space of S^T , its transpose. An orthogonal projection to the column-space of S^T is given by S^+S , and $I - S^+S$ is thus a projection to its orthogonal space. Then

$$\text{FBAPro}(v) = (I - S^+S)v.$$

Equivalently, if $A \in \mathbb{R}^{r \times \dim(\ker(S))}$ is a matrix whose columns form an orthonormal basis of $\ker(S)$, then

$$\text{FBAPro}(v) = (I - S^+S)v = AA^+v = AA^T v,$$

with the last equality following from orthogonality. We will assume here that r and m are asymptotically equivalent (for all metabolic models in BiGG [4], $r/2 \leq m \leq 2r$). Then S^+ can be computed in $O(r^3)$, and either matrix $I - S^+S$ and AA^T can be pre-computed in $O(r^3)$ and applied to multiple inputs. With these precomputed, each application of FBAPro amounts to a matrix-vector multiplication, and thus $\text{FBAPro}(v)$ is fast to apply with a complexity of $O(r^2)$, and is also differentiable and readily parallelized by GPUs. This is in contrast to the linear, quadratic and mixed-integer programming required to solve FBA, MoMA [9] and iMAT [13], respectively, usually solved with optimization algorithms of exponential complexity and lacking a closed-form expression.

FBAPro assumes that all the reference fluxes are relevant but not necessarily exact. We refer to reactions with these assumptions as mid-confidence reactions. One might also be interested in two other assumptions on reactions: high-confidence reactions as ones with exact measured values that we wish to remain fixed after projection to the steady-state space, and unmeasured or low-confidence reactions as ones for which the distance between the input and projected values is irrelevant. Formally, let $L \dot{\cup} M \dot{\cup} H = [r]$ be a partitioning of the reaction indices to low, mid and high confidences. As described next, we introduce variants of FBAPro where some indices are medium confidence, while the rest are either all low confidence or all high confidence.

2.2 FBAproPartial: Ignoring Low Confidence Reactions

For non-empty low confidence indices, we introduce FBAproPartial. For a subset of reaction indices $M = \{m_1, \dots, m_{|M|}\} \subseteq [r]$, let $v^M \in \mathbb{R}^{|M|}$ be the restriction $(v_{m_1}, \dots, v_{m_{|M|}})$. Then we want to compute

$$\text{FBAproPartial}(v, M) := \underset{x \in \text{ker}(S)}{\text{argmin}} \|v^M - x^M\|_2.$$

All indices not in M are treated as low-confidence, and the distance over them is disregarded. While $\|v^M - x^M\|_2$ is the standard Euclidean norm over $\mathbb{R}^{|M|}$, care needs to be taken to ensure an orthogonal projection over these indices corresponds to steady-state solutions. As previously defined, let $A \in \mathbb{R}^{r \times \text{dim}(\text{ker}(S))}$ be such that $\text{col}(A) = \text{ker}(S)$, and let $P^{(M)} \in \{0, 1\}^{|M| \times r}$ be the restriction matrix

$$P_{i,j}^{(M)} = \begin{cases} 1 & j = m_i \\ 0 & \text{otherwise.} \end{cases}$$

$$\text{Claim 2.1. } \text{FBAproPartial}(v, M) = A(P^{(M)}A)^+P^{(M)}v$$

Proof. For convenience, we will denote $P := P^{(M)}$, keeping the dependency on M implicit. For intuition, one can think of a left-multiplication by P as "casting the shadow" of a vector on a lower-dimensional space representing fluxes in the indices in M . Similarly, one can think of PA as the "shadow" of the steady-state space, with a corresponding orthogonal projection $PA(PA)^+$. Our approach is then to map the reference input to the lower dimensional space, project it to the "shadow" of the steady-state, and then find a steady-state vector whose "shadow" we computed. Formally, for any vector $x \in \mathbb{R}^r$, $Px = x^M$, and $A^M := \{x^M | x \in \text{col}(A)\} = \text{col}(PA)$. Then $PA(PA)^+$ is an orthogonal projection from $\mathbb{R}^{|M|}$ to A^M . Therefore,

$$(PA(PA)^+)(Pv) = \underset{y \in A^M}{\text{argmin}} \|y - v^M\|_2. \quad (1)$$

It remains to extend $y \in A^M$ to $x \in \text{col}(A)$. For this, consider the linear equation $y = (PA)z$. A solution for z , if one exists, is given by $z = (PA)^+y$, and $x = Az$ is the corresponding vector in $\text{col}(A)$. Since $A^M = \text{col}(PA)$, we know that such a solution exists for any $y \in A^M$, in particular for $y = (PA(PA)^+)(Pv) = (PA)((PA)^+Pv)$, therefore

$$z = (PA)^+PA(PA)^+(Pv) = (PA)^+Pv$$

is such that PAz solves (1), with the last equality by properties of pseudo-inverse. Note that $PAz = (Az)^M$, and thus

$$\underset{x \in \mathbb{R}^r}{\text{argmin}} \|x^M - v^M\|_2 = Az = A(PA)^+Pv.$$

□

To compute FBAproPartial, one needs to find a linear basis for $\text{ker}(S)$, compute the pseudo-inverse of a matrix with size $\text{dim}(\text{ker}(S)) \times |M|$, and apply a constant amount of matrix multiplication. These operations have a complexity bounded by $O(r^3)$, and they can be precomputed for a fixed set M , with $O(r^2)$ per subsequent application. FBAproPartial thus has the same computational advantages of FBApro.

2.3 FBAproFixed: Fixing High Confidence Reactions

The next case we consider is a partition $M \dot{\cup} H = [r]$ with both M, H being non-empty. For this, we define

$$\text{FBAproFixed}(v, H) := \underset{x \in \text{ker}(S), x^H = v^H}{\text{argmin}} \|v^{[r] \setminus H} - x^{[r] \setminus H}\|_2.$$

We note that given v , the set $L = \{x | x^H = v^H\}$ is an affine space. With the standard basis e_1, \dots, e_r we can express it as $v + \text{span}\{e_i | i \notin H\}$. Denote the matrix with columns $\{e_i | i \notin H\}$ as B . Our problem is then to find an orthogonal projection to

$$L \cap \text{ker}(S) = (v + \text{col}(B)) \cap (\text{col}(A)).$$

Following the notation in [23], we define

$$D = AA^T + BB^T, \quad C = [BB^T D^+ A : AA^T D^+ B]$$

with $:$ denoting concatenation of columns. Then the intersection $L \cap \text{ker}(S)$, if not empty, can be expressed as

$$AA^T D^+ v + \text{col}C.$$

A projection of a vector u to an affine space $x + \text{col}(W)$ is $x + WW^+(u - x)$, and thus the projection of v to $L \cap \text{col}(A)$ is

$$AA^T D^+ v + CC^+(v - AA^T D^+ v) = (CC^+(I - AA^T D^+) + AA^T D^+) v.$$

Note that the affine space L depends on v , but the final expression for the projection is the left-multiplication of v by a matrix dependent only on the set of high confidence indices H . Thus, serendipitously, FBAproFixed can be precomputed and applied as a simple matrix product as the previous variants, with the same complexity.

2.4 Experimental Setup

2.4.1 Methods and Their Inputs

FBA takes as input a metabolic model, specifically a stoichiometric matrix and reaction bounds, as well as a linear objective function, and computes a steady-state flux vector within the reaction bounds maximizing the objective (see Appendix A.1 for details). Both iMAT and MoMA take a metabolic model and a reference vector as input. iMAT interprets the reference vector as representing gene expression (GE), and finds a flux vector with high agreement to the reference vector. MoMA interprets the reference vector as fluxes, and finds the closest steady-state flux vector (see Appendix A.3 for details on both iMAT and MoMA). FBApro receives as input a reference flux, and FBAproFixed, FBAproPartial additionally receive a subset of reactions indices J with higher confidence.

The application of methods to samples in each experiment, then, requires defining an objective, reaction bounds, reference fluxes and higher confidence reactions. We note here that due to technical problems with the implementation of MoMA in Tropo, fixed reaction bounds were used for each model, rather than per sample.

2.4.2 Generating Synthetic Data

To simulate partial noisy flux data, we first retrieved four metabolic models for model organisms from the BiGG Models repository [4] as representatives. We used an *E. coli* model (e_coli_core), a yeast model (iND750), a mouse model (iMM1415) and a human model (Recon1). Let n_t represent the number of reactions in model t . In each experiment, for each model, we compute an orthonormal basis for the steady-state flux space. We then sample 10 random flux vectors for each model (100 for running time experiments), by sampling a linear combination of the basis vectors, with the coefficients independently uniformly distributed in $[0, 1]$. These steady-state vectors, denoted $\{Y_t \in \mathbb{R}^{10 \times n_t} | t \in [4]\}$, represent the hidden ground truth fluxes. Note that the reaction bounds for the models were ignored in this process.

To represent noise in the data, we independently generate factors for each cell in each Y_t , uniformly distributed in a range $[-\delta, \delta]$, denoted Q_t . In the default case, we use $\delta = 1$. We then uniformly sample 10% of the reactions in each model, rounded down, to be the "known" reactions $J_t \subseteq [n_t]$. In the missing/noisy setup, representing approximate partial measurements, we replace the unknown reaction values with zero and apply noise to the rest, resulting in

$$(X_t)_{(i,j)} = \begin{cases} (Y_t)_{(i,j)} \cdot (1 + (Q_t)_{(i,j)}) & j \in J \\ 0 & j \notin J \end{cases} \quad (2)$$

In the noisy/exact setup, we only apply noise to the reactions not in J , resulting in

$$(X_t)_{(i,j)} = \begin{cases} (Y_t)_{(i,j)} & j \in J \\ (Y_t)_{(i,j)} \cdot (1 + (Q_t)_{(i,j)}) & j \notin J \end{cases} \quad (3)$$

These are used as reference fluxes in simulation experiments. We additionally generate data to test the relationship between the performance of the methods and the data generation parameters, namely the magnitude of the multiplicative noise and the fraction of measured reactions. For these simulations, we generate 10 samples for every parameter choice using the human model Recon1. We vary the noise parameter δ with 20 values from 0.01 to 4 while keeping the known reactions fraction $(r - |J|)/r$ at 10%. We then vary the known reaction fraction from 5% to 45%, in 10 steps, keeping δ constant at 1.

2.4.3 Constraining Reaction Bounds for Real Data

We use the Recon1 genome scale human model sourced from BiGG for experiments on NCI60 cancer cell-line data. Instead of the model’s default bounds, we derive feasible reactions flux using Flux Variability Analysis (FVA, see [24, 25] and Appendix A.2). This method constrains the bounds for each reaction to the minimal and maximal flux reachable within a near-optimal FBA solution. We use the dATP demand reaction (id DM_datp_m) as an FBA objective, as the model does not have a biomass reaction, and run FVA with 90% objective optimality and flux loops avoided. We then add (resp., subtract) 10^{-5} to the upper (resp., lower) bounds computed by FVA as a numerical tolerance gap.

2.4.4 Processing CCLE and NCI60 Data

We use metabolite uptake and secretion rate data for NCI60 sourced from [26], matched to existing exchange reactions in the model, as well as intracellular fluxes for two of the cell lines, A549 and MCF7 (originally published in [27], [28] and sourced from [29]), as prediction targets. For each of the two cell lines, we combine the measured exchange and intracellular fluxes to create a reference flux vector. In total, 49 of the reactions had mapped exchange rates. A549 and MCF7 had 28 and 27 reaction flux rates matched to the model, respectively.

We use GE sourced from CCLE [30] (now integrated into TCGA [31]), given in TPM units, for 1378 human cancer cell lines. The data covers both of the aforementioned cell lines, and was matched with 45 cell lines of the NCI60 panel with measured exchange rates. The data was normalized and mapped to the model’s reactions to produce reaction activities in the range $[0, 1]$. These were then mapped to reference fluxes via a linear mapping for each reaction from $[0, 1]$ to the range between its lower and upper bound. See Appendix B for more details on processing GE. Overall, 2200 of the 3741 model reactions were associated with GE data.

2.4.5 Measured Reaction Sets

FBAproFixed and FBAproPartial each require a set of higher confidence reaction indices, high confidence for FBAproFixed and medium confidence for FBAproPartial. For the missing/noisy setup, we use the set of noisy reaction indices as the higher confidence set. For the noisy/exact setup, we use the set of exact reaction indices. For real data, we use the indices of reactions with mapped data, denoted as the measured reaction set.

2.4.6 Sample Specific Reaction Bounds

For FBA and iMAT, we modify the reaction bounds for each sample to fit the reference fluxes. Note that for FBA, this is the only way data is integrated with the method, whereas for iMAT, the reference fluxes are an input as well. Let X be the reference flux matrix for a data source, and J be the measured reaction set. We then define L, U to be the lower and upper bound values for each sample and reaction, of the same size as X . Let δ be an estimation of the noise power in the data. We use a multiplicative window similar to the noise generation for reactions $j \in J$, with

$$\begin{aligned} \forall i. L_{i,j} &= X_{i,j} \cdot (1 - \delta \cdot \text{sign}(X_{i,j})) - 10^{-5} \\ \forall i. U_{i,j} &= X_{i,j} \cdot (1 + \delta \cdot \text{sign}(X_{i,j})) + 10^{-5} \end{aligned}$$

with all reactions not in J using the generic model bounds, modified by FVA for the real data experiments.

For the synthetic data noisy/exact setup, we instead use the aforementioned window for reaction not in J , and a 10^{-5} numerical tolerance window for reactions in J , with

$$L_{i,j} = X_{i,j} - 10^{-5}, \quad U_{i,j} = X_{i,j} + 10^{-5}.$$

For real data, we used $\delta = 1$: given a data value of x , the associated bounds are $(0, 2x)$. Such a large value was chosen to avoid the optimization problem being infeasible for most of the samples, particularly for GE-based data. Infeasible problems still resulted occasionally. We consider this an inherent difficulty of using FBA to fit reference data, and use the solver’s returned solution regardless of the infeasibility for these cases. For simulated data, we used the same noise power parameter used for generating the data.

2.4.7 Model Objective

FBA requires a model objective as an input. For the synthetic data experiments, we use the default objective of the model as stored in BiGG. For the real data experiments, we use the dATP demand reaction of Recon1.

2.4.8 Experiments

For the simulated data, we apply each of the methods to the reference fluxes, sample bounds, objective and measured reaction set J , for every model. We then compare the predictions against ground truth data over the unmeasured reactions, i.e. predictions $Y'_{*,[r]\setminus J}$ and data $Y_{*,[r]\setminus J}$.

For real data, we consider two types of experiments. In the full mapping experiment, we apply the methods to the GE inputs and compare the predictions against flux data, either the NCI60 exchange rates, or the merged NCI60 exchanges and intracellular fluxes for A549 and MCF7. Note that in this kind of experiment, the reference input itself, computed from GE mapped to reaction bounds and a midpoint between bounds for missing data, can be treated as a prediction, denoted as the mid-bound benchmark (see Appendix B). While this is a useful benchmark for predicting real data, note that it does not adhere to the steady-state structure of CBMM, and predicts a constant flux for any unmeasured reaction across all samples.

In the leave-one-out experiment, we apply the methods multiple times on the flux datasets, masking each measured reaction in the reference fluxes and predicting it. Given flux data X and measured reactions J , we define the ground truth $Y = X_{*,J}$. For each $j \in J$, we modify the reference fluxes with $X'_{*,j} = 0$, modify the bounds for reaction j as if it was unmeasured, and fill the column $Y'_{*,j}$ with the output of methods.

2.4.9 Evaluation Metrics

For every experiment, we compare the predictions and target data by computing their Spearman correlations, and their associated p-values. Since both are two-dimensional, we compute correlations per-reaction, with one value per column in the matrices, and per sample, with one value per row. The distribution of correlation coefficients, along with the uncorrected p-values, is analyzed in the results section. Wherever predictions of a method are fixed for a reaction or sample, results for the method are omitted as a conservative comparison, since FBapro variants tend to produce continuous and varying predictions.

2.4.10 Timing

To measure the running time of the different methods over the synthetic data, we first run each method on a random sample for each model. For variants of FBapro, we also test their amortized performance per sample when given the whole matrix X_i as input, for each model i , and additionally when the matrix multiplication takes place on GPU instead of CPU. Finally, we run five replicas for each method call.

2.4.11 System and Software

All time measurements reported in this paper were taken on a node with 1 CPU core, 1 NVIDIA MIG GPU, 32GB of CPU memory and 10 GB of GPU memory, allocated from the Della cluster of Princeton Research Computing.

The code implementing FBapro is available at <https://github.com/Singh-Lab/FBapro>. All code required to reproduce the figures in the paper is available, although the data used must be sourced separately. The repository also contains toy models and examples. All code was written in Python [32]. While many python libraries were used directly and as dependencies, of particular relevance to the method implementations and data processing are COBRApy [19], troppo [33], scipy [34], numpy [35], PyTorch [36], Pandas [37, 38], Seaborn [39] and Matplotlib [40]. Development was primarily done in Pycharm and Jupyter [41].

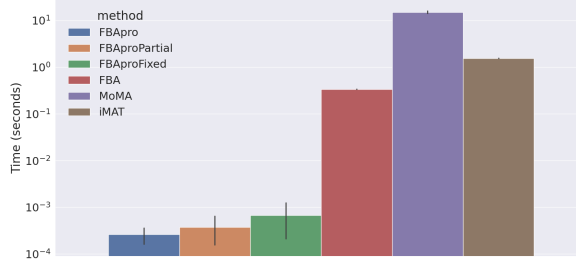


Figure 1: Amortized running time per sample, averaged over five replicas for one sample for benchmark methods, and five replicas for 100 samples for FBapro variants, for different methods on synthetic data generated from four model organism metabolic models.

3 Results

3.1 FBapro is Fast and Scalable

For FBapro to serve as a new, flexible tool in metabolic modeling, it needs to run efficiently. Bulk RNA-seq datasets can contain thousands of samples, and single-cell datasets typically contain tens or hundreds of samples. Moreover, the ability to apply FBA iteratively, as a building block in other algorithms, has contributed to its usefulness throughout the field. Conversely, methods solving a mixed-integer optimization problem (e.g. iMAT) or quadratic optimization problem (e.g. MoMA) are typically run on aggregates of samples representing a condition or group, in part due to their prohibitive running time.

We test the running time of FBapro’s variants on synthetic data, as described in the methods section, and compare it against the running time of FBA, iMAT and MoMA. The results are illustrated in figure 1, run on 100 steady-state samples synthetically generated using the human Recon1 model. Since FBapro and its variants are applied via matrix multiplication, they can be applied to all samples at once on a GPU, and the amortized cost per sample is presented. All variants of FBapro are at least two orders of magnitude faster per application than all optimization-based methods. This relationship is retained across different metabolic models (see appendix, figure 5), and FBapro variants remain at least an order of magnitude faster when running on CPU and/or on smaller or single sample batches (see appendix, figures 6-7). Note that the setup time required to compute the projection matrices is not included in the comparison, as it is typically done once for an experimental setup and can be precomputed, but these are typically on the same order of magnitude as one application of the optimization-based methods (see appendix, figure 8).

3.2 FBapro Recovers Noisy Partial Simulated Data

We next test the ability of FBapro to yield accurate flux predictions given a partially measured reaction set and noisy data, using a generative model for steady-state data applied to four model organism metabolic models sourced from BiGG. We generate data according to two different scenarios. In the missing/noisy data scenario, the values for 90% of the reactions are replaced with zeros, and significant random noise (on the same order of magnitude as the data) is applied to the other 10% before exposing them as inputs to methods. In the exact/noisy data scenario, noise is added to 90% of the reactions, and the other 10% are given as-is to the methods. In both cases, the subset of reactions of higher quality is given as an input to FBapro variants.

Figure 2a shows the Spearman correlations between model outputs and the ground truth on the noisy and missing data, calculated per reaction and per sample. FBapro variants tend to outperform the optimization-based benchmarks, with the exception of FBaproPartial in the exact/noisy experiment. As expected, FBaproPartial is the leading method in the missing/noisy experiment, due to its ability to ignore the values for unmeasured reactions. Similarly, FBaproFixed is the leading method in the exact/noisy experiment (Figure 2b), as it is able to integrate information from all reactions (unlike FBaproPartial) while treating the exactly measured reactions as constraints. FBapro performs consistently well despite its simplicity, with the advantage of not requiring any information about the subset of higher quality reactions. As expected, the missing/noisy experiment is harder, but FBapro is significantly less impacted by the lower quality data than the optimization-based methods. FBA, on the other hand, produces a constant solution for all samples and reactions, and is missing from the correlation plot. Given that the

relationship between methods is similar across the two correlation axes, with sample correlations generally being higher, we focus on sample correlations in the rest of this paper.

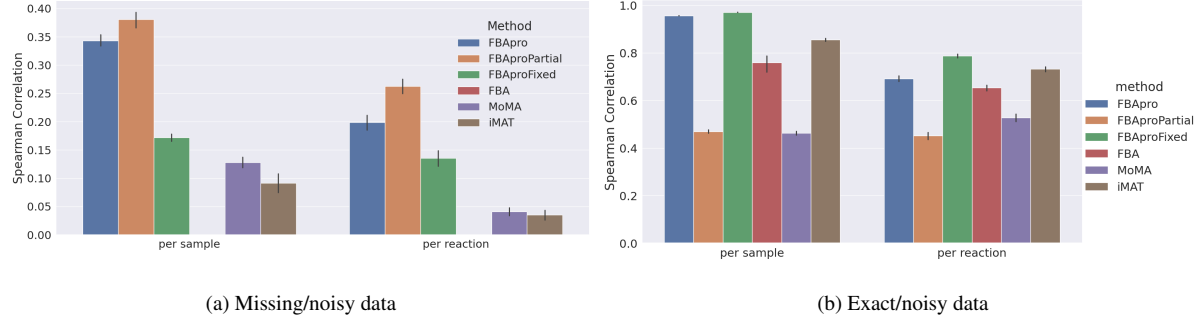


Figure 2: Spearman correlations between actual fluxes and predicted fluxes on synthetic datasets derived from the four model organism metabolic models. **(a)** Average performance across 10 samples for each model and the unmeasured 90% of the model reactions when input data consists of a subset of reactions with noisy flux measurements and the remainder of reactions with no measurements. No data is shown for FBA as it yielded fixed predictions across samples.

(b) Average performance across 10 samples and the noisy 90% of the model reactions when input data consists of fluxes for reactions, a subset with noisy measurements, and the others assumed to be exact measurements.

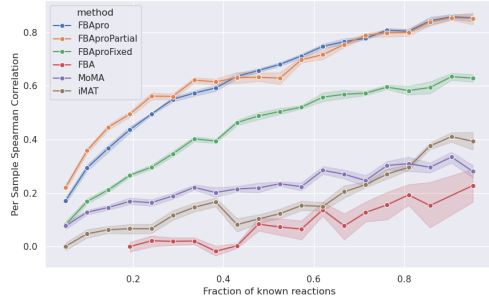
We next vary either the fraction of measured or exact reactions, or the magnitude of noise applied to reactions. Figure 3 shows the per-sample Spearman correlations as a function of the varying parameter. As expected, all methods perform better with less noise and more measured/non-hidden reactions, with the exception of MoMA in one of the experiments. With the exception of FBAProPartial in the noisy-exact setting, all FBAPro variants outperform all other benchmarks across the parameter space except for the extreme noise noisy/exact scenario, where iMAT proves more robust. While real data does not conform to this simplistic model of noise generation, we can infer reasonable expectations for correlations in experiments on real data: Recon1 has 3741 reactions, whereas metabolic measurements typically cover tens to hundreds of reactions/metabolites, amounting to 1-10% of the reactions with the rest missing, while gene expressions can cover significant fractions of the reactions, but carries more noise, confounders and translation challenges. See appendix 9 for per-reaction correlations.

3.2.1 FBAPro Recovers and Predicts Cancer Cell Line Flux Data

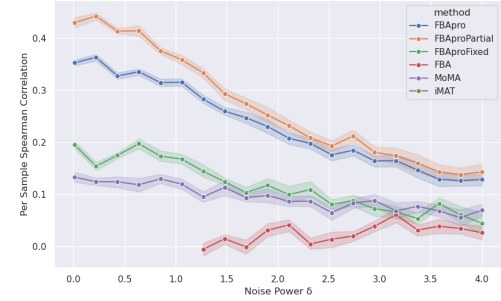
While FBAPro is able to recover noisy partial data in a controlled artificial setting, real metabolic data has many different characteristics. First, the processes introducing noise in real data are mostly unknown and hard to model. Typically, only a very small subset of reactions have associated measurements in an experiment, if any, and the subset is selected in a non-random process (e.g. exchange reactions for small metabolites). More often, reaction fluxes are not directly measured but estimated from other data. The fit between the real metabolic processes and the metabolic model used is also imperfect, adding to the difficulty of mapping measured fluxes to the metabolic model.

We test FBAPro on data from multiple sources for cancer cell lines in the NCI60 panel, and apply all methods using the human Recon1 model. We source exchange rates from [26], intracellular fluxes for two cell lines from [29] (originally [27], [28]), and gene expression for the corresponding cell lines from CCLE ([30]), converted to reaction activities. See section 2.4 for details on data and model processing, as well as method application.

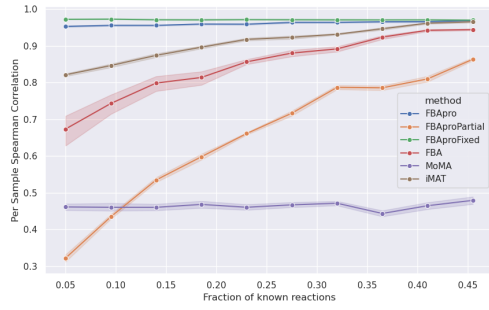
In the first experiment, we follow a leave-one-out approach to test the ability of FBAPro and its variants to recover unmeasured data. We use flux data measured on a small subset of reactions as input, and iteratively mask the fluxes of a single reaction, apply all methods to the input and use the output for the masked reactions as predictions (see section 2.4 for details). The results are shown in Figure 4a. Despite measured reactions used to loosely inform reaction bounds, FBA and iMAT outputs did not significantly correlate with the real fluxes ($p > 0.05$ for all correlations), and an attempt to tighten the bounds they receive as input resulted in an infeasible model. iMAT produced constant predictions across samples and reactions for two of the experiments, and is missing from the correlation plot. FBAPro variants achieve comparatively high correlations. All variants have a significant correlation with A549 fluxes ($p < 0.011$ for all methods), and both FBAProPartial and FBAProFixed have significant correlations with MCF7 fluxes ($p < 1.1 \cdot 10^{-3}$). MoMA performs well on the three data sources, yet is consistently outperformed by both FBAProPartial and FBAProFixed.



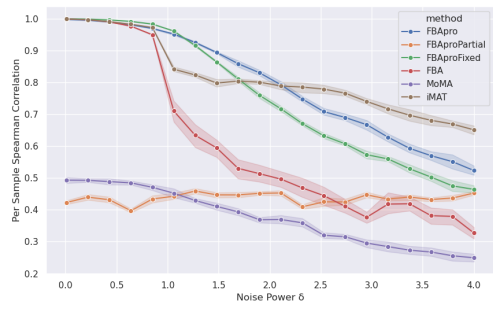
(a) Per sample Spearman correlations in the missing/noisy experiment as a function of the fraction of reactions with measured (though noisy) fluxes. Here, the noise power parameter is set to 1.



(b) Average per sample Spearman correlations in the missing/noisy experiment as a function of the amount of noise added. Here 10% of the reactions have measured (but noisy) fluxes.



(c) Per sample Spearman correlations in the noisy/exact experiment as a function of the fraction of reactions with exact, measured fluxes. The remaining reactions have noisy flux measurements, with the noise power parameter set to 1.

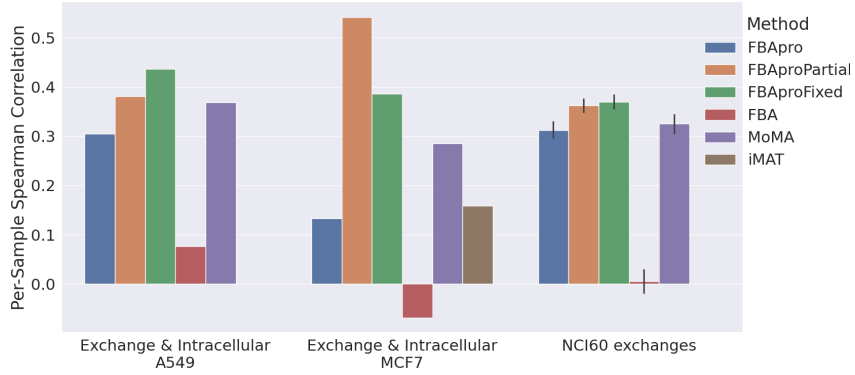


(d) Per sample Spearman correlations in the noisy/exact experiment as a function of the amount of noise added. Here the fraction of reactions with exact flux values given is set to 10%.

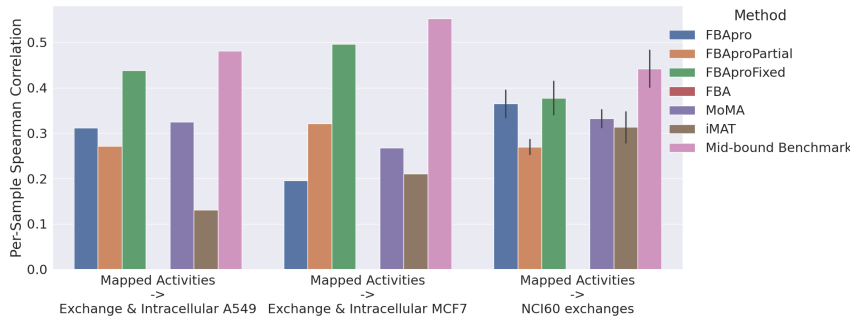
Figure 3: Per sample correlations between model outputs and synthetic data derived from four model organism metabolic models, while varying either the fraction of reactions with measured fluxes or the amount of noise. (3a), (3b) Results for the missing/noisy experiment (where some reactions have no information about fluxes and other reactions have noisy flux measurements). (3c), (3d) Results for the noisy/exact experiment (where some reactions have exact flux measurements and the remaining have noisy flux measurements).

We next test the ability of FBapro and its variants to integrate GE mapped to the model, by applying them to the GE mapped data and comparing their outputs with the corresponding measured fluxes. We convert the GE mapped to reaction activities into flux measures by treating the GE values as defining a point between the lower and upper bound of each reaction, with reactions not covered given the midpoint between their lower and upper bound as a heuristic. This results in an additional benchmark that can be used as comparison, denoted as the Mid-bound benchmark. This simple heuristic turns out to outperform all other methods. However, it does not represent a steady-state flux by itself, which arguably makes it less useful as a tool in real world tasks, for understanding the underlying metabolism informed by the data. Additionally, any reaction without measurements in the data receives a constant prediction across samples for this benchmark, and so it cannot predict relative high or low flux levels for such reactions. Of the other methods, FBA produces constant predictions given GE input, and is missing from the correlation plot. All other methods have significant correlations (mean uncorrected p-value < 0.05 in the case of NCI60 samples), with the exception of FBaproPartial on NCI60 (mean uncorrected p-value > 0.05), FBapro and iMAT on MCF7 and iMAT on A549. FBaproFixed overperforms all other steady-state methods across the data sources.

Overall, FBapro, and in particular its modifications, achieve significant and moderate correlations with flux data for both flux and GE input across most experiments. Given the fraction of measured fluxes in the leave-one-out experiment, and the loose expected relation between GE and reactions in the mapping experiments, the correlations are higher than expected based on the simulated data.



(a) Leave-one-out experiments, where the flux for one measured reaction is masked out and the remaining fluxes are given to the methods as input. Spearman correlations between the fluxes output by the methods and the masked experimentally-measured reaction fluxes, grouped by data source. For the NCI60 exchanges, average per-sample correlations across the 45 cell lines with measured exchanges are given, with 95% confidence intervals.



(b) Full mapping experiments, where GE is mapped to reaction activities and is given as input to the methods. Spearman correlations between methods applied to the input and actual flux measurements for these sample, grouped by input and target data. The Mid-Bound benchmark does not yield steady state predictions, and reflects the quality of the initial GE mapped activities and the model’s reaction bounds. For the NCI60, average per-sample correlations across the 45 cell lines with measured exchanges are given, with 95% confidence intervals. FBA performance is not shown as it yielded constant flux predictions, indicating the difficulty in translating GE to feasible, meaningful flux bounds for FBA.

Figure 4: Performance of methods when predicting fluxes from GE data and masked flux data.

4 Discussion

In this work we present FBAPro, a simple linear transformation solving the problem of finding a closest steady-state flux to a reference flux vector. We demonstrate that FBAPro is computationally scalable to large amounts of data, allowing a qualitative difference in the kinds of data and *in vitro* experiments that can be utilized with it. FBAPro also performs on par or better than existing methods in denoising and recovering missing data, as well as on predicting fluxes based on GE. We further show how FBAPro can be extended and modified, similarly to FBA, by introducing FBAProFixed and FBAProPartial, each tailored to excel in a specific use case.

A major factor of the centrality of FBA in metabolic modeling is the ease with which it can be modified, resulting in a wide variety of methods in the field extending the optimization problem or utilizing FBA as a building block within their algorithm. We believe that FBAPro, as another simple, flexible method, can also serve as another basic building block and inspire more diverse future methods.

One of the motivating reasons for substituting a linear transformation for linear programming is that this closed-form differentiable function can fit within a gradient-learning framework. We believe FBAPro has the potential to improve such frameworks applied to metabolic modeling, either as a concept bottleneck preventing overfitting, or as a mechanism for transfer learning by constraining an inner layer to have a structure interpretable as reaction fluxes. While machine learning frameworks have yielded breakthrough advances in multiple sequence-related biological tasks, they have not achieved the same level of success within CBMM. We believe that more domain-specific modules compatible with machine learning frameworks—such as FBAPro—may be a help in bridging

this gap.

5 Acknowledgments

Simulations presented in this article were performed on computational resources managed and supported by Princeton Research Computing resources at Princeton University, as well as the Lewis-Sigler Institute Computational Resources.

References

- [1] Eleftherios Terry Papoutsakis and Charles L Meyer. Equations and calculations of product yields and preferred pathways for butanediol and mixed-acid fermentations. *Biotechnology and bioengineering*, 27(1):50–66, 1985.
- [2] Jeffrey D Orth, Ines Thiele, and Bernhard Ø Palsson. What is flux balance analysis? *Nature biotechnology*, 28(3):245–248, 2010.
- [3] David A Fell and J Rankin Small. Fat synthesis in adipose tissue. an examination of stoichiometric constraints. *Biochemical journal*, 238(3):781–786, 1986.
- [4] Charles J Norsigian, Neha Pusarla, John Luke McConn, James T Yorkovich, Andreas Dräger, Bernhard O Palsson, and Zachary King. Bigg models 2020: multi-strain genome-scale models and expansion across the phylogenetic tree. *Nucleic Acids Research*, 48(D1):D402–D406, 11 2019.
- [5] Jeremy S Edwards, Markus Covert, and Bernhard Palsson. Metabolic modelling of microbes: the flux-balance approach. *Environmental microbiology*, 4(3), 2002.
- [6] Karthik Raman and Nagasuma Chandra. Flux balance analysis of biological systems: applications and challenges. *Briefings in bioinformatics*, 10(4):435–449, 2009.
- [7] Michael Kohlstedt, Judith Becker, and Christoph Wittmann. Metabolic fluxes and beyond—systems biology understanding and engineering of microbial metabolism. *Applied microbiology and biotechnology*, 88(5):1065–1075, 2010.
- [8] Nathan E Lewis, Harish Nagarajan, and Bernhard O Palsson. Constraining the metabolic genotype–phenotype relationship using a phylogeny of in silico methods. *Nature Reviews Microbiology*, 10(4):291–305, 2012.
- [9] Daniel Segre, Dennis Vitkup, and George M Church. Analysis of optimality in natural and perturbed metabolic networks. *Proceedings of the national academy of sciences*, 99(23):15112–15117, 2002.
- [10] Tomer Shlomi, Omer Berkman, and Eytan Ruppin. Regulatory on/off minimization of metabolic flux changes after genetic perturbations. *Proceedings of the national academy of sciences*, 102(21):7695–7700, 2005.
- [11] Daniel J Cook and Jens Nielsen. Genome-scale metabolic models applied to human health and disease. *Wiley Interdisciplinary Reviews: Systems Biology and Medicine*, 9(6):e1393, 2017.
- [12] Scott A Becker and Bernhard O Palsson. Context-specific metabolic networks are consistent with experiments. *PLoS computational biology*, 4(5):e1000082, 2008.
- [13] Tomer Shlomi, Moran N Cabili, Markus J Herrgård, Bernhard Ø Palsson, and Eytan Ruppin. Network-based prediction of human tissue-specific metabolism. *Nature biotechnology*, 26(9):1003–1010, 2008.
- [14] Livnat Jerby, Tomer Shlomi, and Eytan Ruppin. Computational reconstruction of tissue-specific metabolic models: application to human liver metabolism. *Molecular systems biology*, 6(1):401, 2010.
- [15] Rasmus Agren, Sergio Bordel, Adil Mardinoglu, Natapol Pornputtapong, Intawat Nookaew, and Jens Nielsen. Reconstruction of genome-scale active metabolic networks for 69 human cell types and 16 cancer types using init. *PLoS computational biology*, 8(5):e1002518, 2012.
- [16] Allon Wagner, Chao Wang, Johannes Fessler, David DeTomaso, Julian Avila-Pacheco, James Kaminski, Sarah Zaghouani, Elena Christian, Pratiksha Thakore, Brandon Schellhaass, et al. Metabolic modeling of single th17 cells reveals regulators of autoimmunity. *Cell*, 184(16):4168–4185, 2021.
- [17] John Jumper, Richard Evans, Alexander Pritzel, Tim Green, Michael Figurnov, Olaf Ronneberger, Kathryn Tunyasuvunakool, Russ Bates, Augustin Åde, Anna Potapenko, Alex Bridgland, Clemens Meyer, Simon A. A. Kohl, Andrew J. Ballard, Andrew Cowie, Bernardino Romera-Paredes, Stanislav Nikolov, Rishabh Jain, Jonas Adler, Trevor Back, Stig Petersen, David Reiman, Ellen Clancy, Michal Zielinski, Martin Steinegger, Michalina Pacholska, Tamas Berghammer, Sebastian Bodenstein, David Silver, Oriol Vinyals, Andrew W. Senior, Koray Kavukcuoglu, Pushmeet Kohli, and Demis Hassabis. Highly accurate protein structure prediction with AlphaFold. *Nature*, 596(7873):583–589, 2021.

- [18] Sean R Hackett, Vito RT Zanotelli, Wenxin Xu, Jonathan Goya, Junyoung O Park, David H Perlman, Patrick A Gibney, David Botstein, John D Storey, and Joshua D Rabinowitz. Systems-level analysis of mechanisms regulating yeast metabolic flux. *Science*, 354(6311):aaf2786, 2016.
- [19] Ali Ebrahim, Joshua A Lerman, Bernhard O Palsson, and Daniel R Hyduke. Cobrapy: constraints-based reconstruction and analysis for python. *BMC systems biology*, 7:1–6, 2013.
- [20] Markus W Covert, Christophe H Schilling, and Bernhard Palsson. Regulation of gene expression in flux balance models of metabolism. *Journal of theoretical biology*, 213(1):73–88, 2001.
- [21] Joshua AM Kaste and Yair Shachar-Hill. Accurate flux predictions using tissue-specific gene expression in plant metabolic modeling. *Bioinformatics*, 39(5):btad186, 2023.
- [22] Daniel Machado and Markus Herrgård. Systematic evaluation of methods for integration of transcriptomic data into constraint-based models of metabolism. *PLoS computational biology*, 10(4):e1003580, 2014.
- [23] & Odell P. L. Piziak R. Affine projections. *Computers and Mathematics with Applications*, 2004.
- [24] Anthony P Burgard, Shankar Vaidyaraman, and Costas D Maranas. Minimal reaction sets for escherichia coli metabolism under different growth requirements and uptake environments. *Biotechnology progress*, 17(5):791–797, 2001.
- [25] Radhakrishnan Mahadevan and Chrisophe H Schilling. The effects of alternate optimal solutions in constraint-based genome-scale metabolic models. *Metabolic engineering*, 5(4):264–276, 2003.
- [26] M. Jain, R. Nilsson, S. Sharma, N. Madhusudhan, T. Kitami, A.L. Souza, and V.K. Mootha. Metabolite profiling identifies a key role for glycine in rapid cancer cell proliferation. *Science*, 336(6084):1040–1044, 2012.
- [27] Christian M Metallo, Jason L Walther, and Gregory Stephanopoulos. Evaluation of ¹³C isotopic tracers for metabolic flux analysis in mammalian cells. *Journal of biotechnology*, 144(3):167–174, 2009.
- [28] Neil S Forbes, Adam L Meadows, Douglas S Clark, and Harvey W Blanch. Estradiol stimulates the biosynthetic pathways of breast cancer cells: detection by metabolic flux analysis. *Metabolic engineering*, 8(6):639–652, 2006.
- [29] Daniel C. Zielinski, Neema Jamshidi, Amanda J. Corbett, Aarash Bordbar, Allison Thomas, and Bernhard ø. Palsson. Systems biology analysis of drivers underlying hallmarks of cancer cell metabolism. *Scientific Reports*, 7(1):41241, 2017.
- [30] Jordi Barretina, Giordano Caponigro, Nicolas Stransky, Kavitha Venkatesan, Adam A Margolin, Sungjoon Kim, Christopher J Wilson, Joseph Lehár, Gregory V Kryukov, Dmitriy Sonkin, et al. The cancer cell line encyclopedia enables predictive modelling of anticancer drug sensitivity. *Nature*, 483(7391):603–607, 2012.
- [31] National Cancer Institute. The cancer genome atllast program (tcga). <https://www.cancer.gov/tcga>. Accessed: 2025-12-11.
- [32] Guido Van Rossum and Fred L. Drake. *Python 3 Reference Manual*. CreateSpace, Scotts Valley, CA, 2009.
- [33] Jorge Ferreira, Vítor Vieira, Jorge Gomes, Sara Correia, and Miguel Rocha. Troppo-a python framework for the reconstruction of context-specific metabolic models. In *Practical Applications of Computational Biology and Bioinformatics, 13th International Conference*, pages 146–153. Springer, 2020.
- [34] Pauli Virtanen, Ralf Gommers, Travis E. Oliphant, Matt Haberland, Tyler Reddy, David Cournapeau, Evgeni Burovski, Pearu Peterson, Warren Weckesser, Jonathan Bright, Stéfan J. van der Walt, Matthew Brett, Joshua Wilson, K. Jarrod Millman, Nikolay Mayorov, Andrew R. J. Nelson, Eric Jones, Robert Kern, Eric Larson, C J Carey, İlhan Polat, Yu Feng, Eric W. Moore, Jake VanderPlas, Denis Laxalde, Josef Perktold, Robert Cimrman, Ian Henriksen, E. A. Quintero, Charles R. Harris, Anne M. Archibald, Antônio H. Ribeiro, Fabian Pedregosa, Paul van Mulbregt, and SciPy 1.0 Contributors. SciPy 1.0: Fundamental Algorithms for Scientific Computing in Python. *Nature Methods*, 17:261–272, 2020.

- [35] Charles R. Harris, K. Jarrod Millman, Stéfan J. van der Walt, Ralf Gommers, Pauli Virtanen, David Cournapeau, Eric Wieser, Julian Taylor, Sebastian Berg, Nathaniel J. Smith, Robert Kern, Matti Picus, Stephan Hoyer, Marten H. van Kerkwijk, Matthew Brett, Allan Haldane, Jaime Fernández del Río, Mark Wiebe, Pearu Peterson, Pierre Gérard-Marchant, Kevin Sheppard, Tyler Reddy, Warren Weckesser, Hameer Abbasi, Christoph Gohlke, and Travis E. Oliphant. Array programming with NumPy. *Nature*, 585(7825):357–362, September 2020.
- [36] Adam Paszke, Sam Gross, Francisco Massa, Adam Lerer, James Bradbury, Gregory Chanan, Trevor Killeen, Zeming Lin, Natalia Gimelshein, Luca Antiga, et al. Pytorch: An imperative style, high-performance deep learning library. *Advances in neural information processing systems*, 32, 2019.
- [37] The pandas development team. pandas-dev/pandas: Pandas, February 2020.
- [38] Wes McKinney. Data Structures for Statistical Computing in Python. In Stéfan van der Walt and Jarrod Millman, editors, *Proceedings of the 9th Python in Science Conference*, pages 56 – 61, 2010.
- [39] Michael L. Waskom. seaborn: statistical data visualization. *Journal of Open Source Software*, 6(60):3021, 2021.
- [40] J. D. Hunter. Matplotlib: A 2d graphics environment. *Computing in Science & Engineering*, 9(3):90–95, 2007.
- [41] Thomas Kluyver, Benjamin Ragan-Kelley, Fernando Pérez, Brian Granger, Matthias Bussonnier, Jonathan Frederic, Kyle Kelley, Jessica Hamrick, Jason Grout, Sylvain Corlay, Paul Ivanov, Damián Avila, Safia Abdalla, Carol Willing, and Jupyter development team. Jupyter notebooks - a publishing format for reproducible computational workflows. In Fernando Loizides and Birgit Scmidt, editors, *Positioning and Power in Academic Publishing: Players, Agents and Agendas*, pages 87–90, Netherlands, 2016. IOS Press.
- [42] Miha MoÅ¡kon and Tadeja ReÅ¡en. Context-specific genome-scale metabolic modelling and its application to the analysis of covid-19 metabolic signatures. *Metabolites*, 13(1), 2023.

Appendix A Background

A.1 Constraint-Based Metabolic Modeling and Flux Balance Analysis

Let $S \in \mathbb{R}^{m \times r}$ be a stoichiometric matrix whose rows correspond to metabolites and columns to reactions. The value of $S_{i,j}$ represents the concentration (or amount) of metabolite i (e.g. in micromolar units μM) produced (or consumed, if negative) by one unit of flux of reaction j , in inverse time unit (e.g. $1/sec$). Given a vector of flux rates $v \in \mathbb{R}^r$, the vector $Sv \in \mathbb{R}^m$ represents the rate of change in each metabolite. The steady-state assumption at the heart of CBMM is then $Sv = 0$.

FBA aims to simulate the fluxes in the cell (or tissue, organism, community) that S represents, under the assumption that metabolic processes aim to maximize a linear objective in terms of reaction fluxes $c \in \mathbb{R}^r$. Typically, c represents growth, by giving a positive coefficient to a reaction representing the consumption of different metabolites for the creation of biomass. The objective value for a flux vector v is then $c^T v$. Since the objective is linear, any v with nonzero objective value can be arbitrarily scaled to achieve any objective value. Therefore, CBMM adds constraints to the fluxes of each reaction preventing arbitrary scaling, and potentially encoding real biological constraints of reaction direction, enzyme abundance or metabolite availability. Let $lb, ub \in \mathbb{R}^r$ be vectors representing the lower and upper bounds for reaction fluxes, respectively. FBA is the linear program solving for an optimal flux vector, that is

$$\begin{array}{ll} \max_v & c^T v \\ \text{subject to} & \begin{array}{l} Sv = 0 \\ v \leq ub \\ v \geq lb. \end{array} \end{array}$$

A.2 Flux Variability Analysis

Flux Variability Analysis (FVA) is a method used to automatically adjust the bounds of a reactions in a model to represent their feasible flux ranges. Intuitively, every solution to FBA, for a non-degenerate model, has critical inequalities that are satisfied in an equation in that solution. However, an inequality may remain unsatisfied in any optimal (or near-optimal) solution, e.g. an upper bound on reactions involved in glycolysis may be higher than the maximal rate of uptake and production of glucose in the model. FVA aims to replace reaction bounds such that each one has a near-optimal solution in which it is critical.

Formally, let $\alpha \in [0, 1]$ be a fraction of optimality, and c, S, lb, ub as in the formulation of FBA, and x be the optimal value of FBA's objective. Then for every reaction j , FVA computes

$$\begin{array}{ll} lb_j^* = \min_v & v_j \\ \text{subject to} & \begin{array}{l} Sv = 0 \\ c^T v \geq \alpha x \\ v \leq ub \\ v \geq lb, \end{array} \end{array}$$

and similarly ub_j^* with maximization substituted for minimization. This amounts to two FBA-like linear programs run for each reaction in the model.

A common modification to FVA is to solve the aforementioned program with the added requirement of no flux loops, also known as futile cycles or thermodynamically infeasible cycles. These are typically defined as flux vectors with non-zero fluxes only for mass-preserving reactions, and no exchange or demand reactions.

A.3 Context-Specific CBMM Methods

Many methods have been developed to simulate the metabolism of systems under a specific context. Such a context can be a gene knock-out strain, a specific growth medium, measured fluxes of gene expression. We cover

two such methods here. Minimization of Metabolic Adjustment (MoMA) receives as input a metabolic model with stoichiometry S and bounds lb, ub , and a reference flux v . While the method is generic, the original and still standard implementation is in the context of a knock-out strain, where v is taken from a wild-type model, whereas S represents some subset of the original model's reactions. MoMA is then the quadratic program

$$\begin{array}{ll} \min_x & \| v - x \|_2^2 \\ \text{subject to} & Sx = 0 \\ & x \leq ub \\ & x \geq lb. \end{array}$$

Integrative Metabolic Analysis Tool (iMAT) is designed to simulate reaction fluxes given GE input. Assume the GE has been mapped to reactions resulting in a reference vector v as in MoMA, albeit with nonnegative values. However, given the inherent noise and loose relationship between genes and reaction fluxes, iMAT interprets the reference vector as indicating only which reactions are likely active and which ones aren't. Let $a, b \in [0, 1]$ be fixed thresholds for interpreting active and inactive indications. Let x be the percentile ranks of the values of v , such that $x_i \in [0, 1]$ represents the fraction of reactions with lower values, or $|\{j|v_j \leq v_i\}| / r$. Then the reactions of the models are partitioned to $L = \{i|x_i < a\}$, $H = \{i|x_i > b\}$, M otherwise. Presented verbally and simplified here, iMAT is the mixed-integer program maximizing the number of reactions in H with non-trivial flux, and the number of reactions in L with zero flux, conforming to steady-state assumptions. For our experiments, we used $a = 1/3, b = 2/3$.

Appendix B Processing and Mapping Gene Expression to Reference Fluxes

GE datasets are processed as follows: Genes with less than 15% non-zero values across samples are dropped. We then apply a quantile transformation to the expression data: denote the number of genes as g . We first create a reference distribution by taking, for every rank $i \leq g$, the mean expression value of the i 'th smallest value in each sample. We then map the values of each sample to this distribution, preserving their ranking. The entire GE matrix is then shifted and scaled so that the values are in the range $[0, 1]$, to represent relative activity.

In order to apply any method to GE data, it must be mapped from the gene space to the reaction space of the model. We follow a typical process for the mapping, although the implementation details are not standardized in the literature [42]. We use the model's Gene-Protein-Reaction (GPR) association, which associates each reaction with a logical expression with gene ids as variables. In the case of multiple transcript variants in the model, this information is ignored for matching with GE data. The logical operators AND and OR are replaced with geometric mean and arithmetic mean, respectively, and the GE values are substituted for the variables to result in raw reaction activities. Genes not in the data are ignored, so means are taken over the rest. Note that this preserves the range of the GE values.

Let lb, ub denote the upper and lower bounds of a reaction, and x denote its activity in a sample. For a forward reaction, with $lb, ub \geq 0$, the corresponding reference flux is $lb + x(ub - lb)$, such that an activity of 0 corresponds to lb and 1 to ub . For backward reactions with $lb, ub \leq 0$, the roles of lb, ub are reversed in the mapping. For reversible reactions with $lb \leq 0 \leq ub$, no value is assigned from activity. These, as well as reactions without a GPR, or without any matching genes in the data, are assigned a reference flux of $(lb + ub)/2$. Note that after running FVA only a small fraction of the reactions remain bidirectional (323/3418).

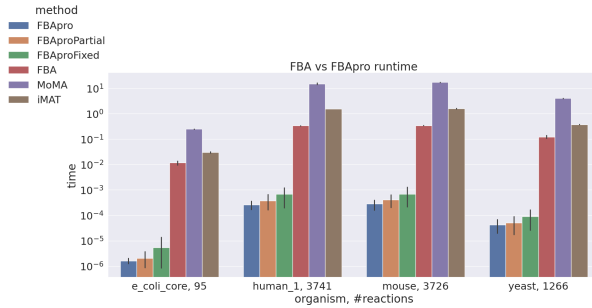


Figure 5: Running time of methods on synthetic data for four model organism models

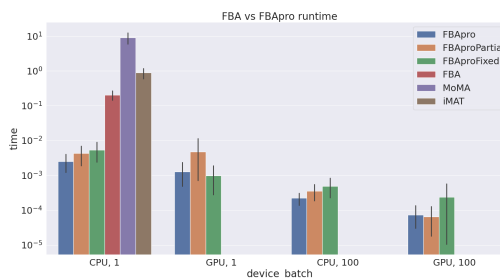


Figure 6: Running time of methods on different devices and batch sizes (when applicable), synthetic data on Recon1

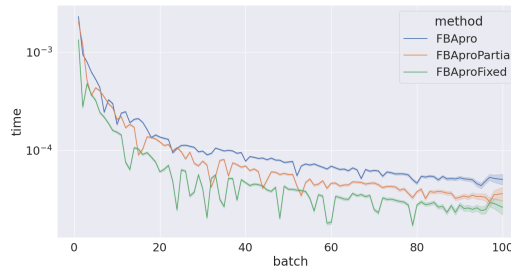


Figure 7: Running time of FBapro variants as a function of batch sizes on GPU synthetic data on Recon1

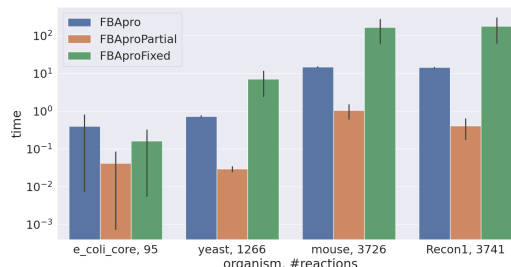
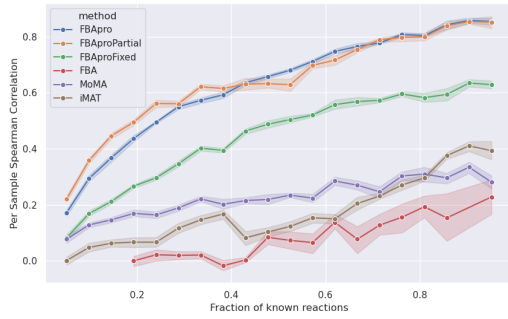
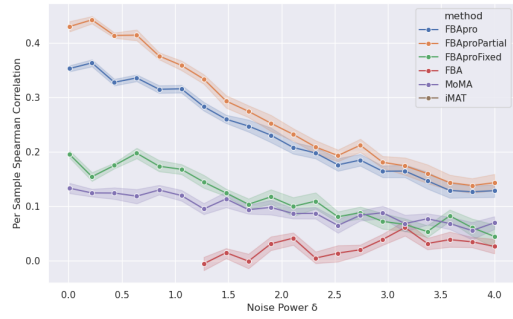


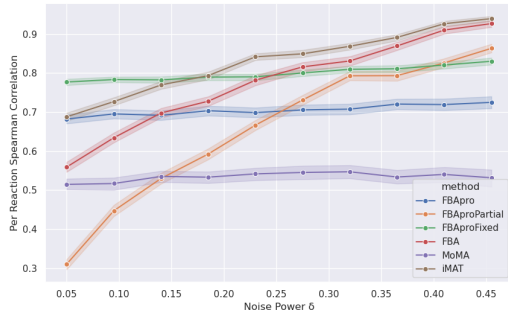
Figure 8: Time for setup



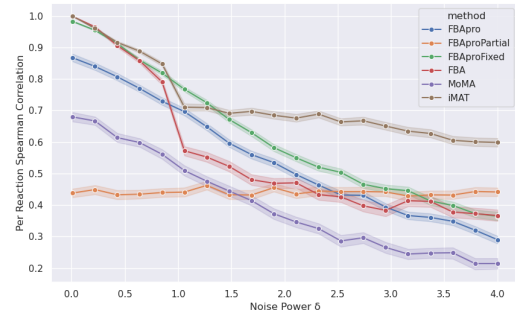
(a) Per reaction Spearman correlations, missing/noisy experiment, function of fraction of noisy reactions



(b) Per reaction Spearman correlations, missing/noisy experiment, function of noisy power



(c) Per reaction Spearman correlations, noisy/exact experiment, function of fraction of exact reactions



(d) Per reaction Spearman correlations, noisy/exact experiment, function of noise power

Figure 9: Per reaction correlations between model outputs and synthetic data on Recon1, while varying the fraction of known reactions or power of noise. 9a and 9b show the missing/noisy experiment, whereas 9c and 9d show the noisy/exact experiment